applied sciences

MDPI

Article

Cooperative Standoff Tracking of Moving Targets Using Modified Lyapunov Vector Field Guidance

Fei Che, Yifeng Niu, Jie Li and Lizhen Wu *

College of Intelligence Science and Technology, National University of Defense Technology, Changsha 410073, China; chefei1013@163.com (F.C.); niuyifeng@nudt.edu.cn (Y.N.); leonlee2009@163.com (J.L.)

* Correspondence: lzwu@nudt.edu.cn

Received: 5 May 2020; Accepted: 25 May 2020; Published: 27 May 2020

Abstract: Cooperative standoff tracking of moving targets is an important application of fixed-wing unmanned aerial vehicles (UAVs). To cope with the problem of long convergence time and unstable tracking in cooperative target tracking, traditional Lyapunov vector field guidance (LVFG) is modified. The guidance parameter c is discussed, and the gradient descent method is utilized to develop the optimal guidance parameter search algorithm. As for tracking moving targets, an interacting multiple model-based unscented Kalman filter (IMM-UKF) estimator is built for predicting the target state, and the result is used for correcting the guidance law. Meanwhile, a speed-based controller is developed for faster convergence to the desired intervehicle phase, and the stability of the controller is proved using the Lyapunov stability theory. Numerical simulation results indicate the proposed guidance converges faster to the standoff circle without intersecting the orbit. The state estimator reduces the estimate error and the intervehicle phase converges faster to the desired phase than the traditional control method. Furthermore, extensive hardware-in-the-loop simulations are carried out to verify the feasibility of the algorithm.

Keywords: standoff tracking; cooperative tracking; moving target; vector field guidance; IMM-UKF; phase keeping

1. Introduction

Fixed-wing unmanned aerial vehicles (UAVs) have been widely used in area surveillance, convoy protection, coordinate combat, and forest firefighting. One of the main applications is cooperative standoff "targets" tracking, usually a vehicle on the ground, static or moving. To render the problem feasible, there is a need to divide it into three subproblems. The first subproblem is to generate the optimal flyable path for a single UAV where UAVs should follow in order to achieve stable standoff tracking of static targets. In the standoff tracking approach, UAVs should stably keep an appropriate distance from the target. The next component is concerned with standoff tracking of moving targets, mainly the states (location and velocity) estimation of the target, which could help modify the guidance law for a moving target. However, it is usually ignored in many researches. The last subproblem is the coordination of a team of UAVs, mainly keeping a fixed intervehicle phase. The three subproblems are interrelated and they should be solved simultaneously.

Tremendous research efforts have been made in order to generate the optimal path for a single UAV. The guidance laws are usually based on several approaches: Helmsman behavior control [1], model prediction control [2,3], reference point control [4,5], and vector field guidance. As a classic guidance law, Lyapunov vector field guidance (LVFG) has been improved up to now. It is in a decoupled structure in which the rate of heading and speed change are separately controlled for standoff distance and phase angle keeping. Dale L et al. [6] introduced the Lyapunov vector field into

the loitering algorithm for standoff tracking. Frew E.W et al. [7] extended single UAV tracking to cooperative tracking. To shorten the convergence time, Chen H et al. [8] combined the tangent with the Lyapunov vector field guidance and Oh H et al. [9] used the tangent vector field in conjunction with the sliding mode control that is modified by introducing additional adaptive terms. Besides integrating control methods into vector field, Lim S et al. [10] added a new non-dimensional parameter c into original algorithm, adjusting the convergence time to standoff circle by changing c and in this way, arrival position and time are controlled. Aiming to limit the UAV turn rate within the capability imposed by the angle limits, Pothen A et al. [11] transformed c to a simple function of R, orbit radius. Shun Sun et al. [12] analyzed the criteria guidance term c should fulfill, proposed a series of guidance functions satisfying the conditions, and an offline parameter search algorithm was designed for selecting the optimal function, while flexibility is limited. The methods mentioned above mainly concern themselves with converging to the standoff distance at the highest speed and keeping it steady, but they cannot address the fast convergence and stable tracking simultaneously.

When tracking a ground moving target, the UAVs need to modify the guidance laws using the state of the target. The access to the location and velocity of the target is of vital importance to standoff tracking. In the past research of guidance laws in standoff tracking, some researchers [5,7,13,14] simplify the problem by assuming that the state of the target is available. They assumed that the state of the target can be obtained via direct communication with a cooperative ground vehicle, or continuous data for the target state are used in experiments. It is obviously not realistic when tracking an uncooperative target. Other researchers take tighter experimental conditions into consideration. In Seungkeun Kim's research [2], the state-vector fusion based on the extend Kalman filter (EKF) was utilized to estimate the state of the moving target for two UAVs. Summers T.H et al. [15] took unknown wind and target motions into one variable and proposed an adaptive estimator for a more accurate estimation of the unknown factor. A jerk model for tracking highly maneuvering targets was utilized in Qian Z's work [16]. In cooperative tracking of the moving target, Hu C. et al. [17] applied squared-root cubature information filtering for data processing from four quadrotor UAVs, and the consensus algorithm is used in order to improve estimation accuracy. The methods mentioned above mostly cannot estimate the state of a maneuvering target satisfactorily or are not suitable for fixed-wing UAVs.

Due to the poor estimation of target position and velocity by a single UAV, a team of UAVs for cooperative standoff tracking are imperative. Kingston D et al. [18] introduced an orbit radius change method without velocity control for phase keeping of multiple UAVs. Frew E W et al. [7] proposed a guidance law that adjusts the speed of vehicle to maintain the desired relative phase on the loiter circle, which is adopted in phase separation of multiple UAVs by many researchers [2,15,16]. Song Z Q et al. [19] added a second derivative term to the speed controller for phase keeping. Oh H et al. [9] realized the angular separation control by changing velocity or orbit radius in different information structures. Kokolakis N M T et al. [20] extended the phase separation problem to tracking a moving target, focusing simultaneously on convergence toward the standoff radius, heading, and angular difference. Lim S et al. [10] controlled the arrival position on the desired circle by adjust the parameter c, and changed the desired radius and vehicle speed to keep a certain phase between UAVs. He S et al. [21] adopted a new leader–follower information architecture and an acceleration for space angle control. Xu Z [5] newly developed the predicted reference point guidance method to reduce errors in standoff distance and phase angle control. Different methods are utilized to keep a fixed phase between neighboring UAVs, but the inter-vehicle phase cannot converge to the desired phase in finite time, which is harmful for cooperative tracking of a moving target.

Although significant and constructive research efforts have been performed, stable standoff tracking of uncooperative moving target by a team of UAVs has not yet been addressed properly. It is also a challenge to balance converging speed and stability of tracking, and the estimation of target states with less prior information still needs to be improved, which is of vital important to tracking moving targets. For cooperative tracking, faster settling down to the desired position helps more stable tracking.

Carrying out this study, we hope to deal with the three subproblems better, which means guiding UAVs to tracking target in a faster converging time, getting a more accurate estimation of target state, and making intervehicle phase converge to the desired value in a shorter time.

This paper's principal contributions can be summarized as follows: Taking the trajectory curvature into consideration, an optimization algorithm based on the gradient descent method for searching the optimal guidance parameter c is developed, which means faster convergence and stable tracking can be guaranteed. When UAVs are tracking a moving target, an interacting multiple model based on unscented Kalman filter (IMM-UKF) estimator is built for predicting the target state. In this way, the stability of the uncooperative target is improved. For cooperative tracking, a new speed control-based phase-keeping controller is designed to achieved faster convergence to the desired intervehicle phase, and the stability of controller is proved.

The remainder of the paper is organized as follows: Section 2 mainly introduces the problems to be handled with. In Section 3, the overall framework of the LVFG algorithm is presented, and two components of guidance are analyzed. The proposed solution is introduced in Section 4, and fast but stable tracking, estimator for target states, and phase-keeping controller are presented. To verify the feasibility and benefits of our methods, numerical simulation and Hardware-In-the-Loop (HIL)simulation are conducted, of which the results are presented in Section 5, and the conclusions are described in Section 6.

2. Problem Statement

2.1. Standoff Tracking

A fixed-wing UAV cruising at a constant speed and fixed altitude is used to track a target on the ground, as shown in Figure 1. Assuming that the position vector of the UAV is $(x_{uav}, y_{uav})^T$ in a frame with the target at $(x_{target}, y_{target})^T$, and the position of the UAV in the local coordinate system of the target can be expressed as $(x_r, y_r)^T$, or in the local polar coordinate system as (r, θ):

$$\begin{cases} r=\sqrt{x_r{}^2+y_r{}^2} \\ \theta=a\tan(y_r/x_r) \end{cases} \tag{1}$$

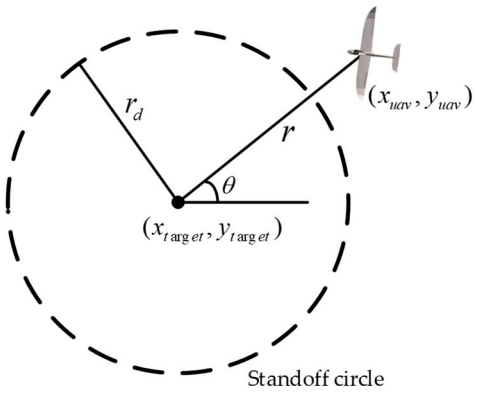

Figure 1. Scenario of standoff target tracking.

In the tracking process, the kinematic model of the constant-speed UAV can be presented as:

$$\begin{cases} \dot{x}_{uav}=s(t)\cdot\cos(\psi(t)) \\ \dot{y}_{uav}=s(t)\cdot\sin(\psi(t)) \\ \dot{\psi}=k(\psi_d-\psi) \end{cases} \tag{2}$$

where $s(t)$ is the UAV speed, and ψ_d is the desired course. We guide the UAV toward the standoff circle by control ψ_d. In the process, $\triangle r = r - r_d$ converges to zero.

2.2. Phase Keeping

When a team of UAVs are utilized to track the ground target in a cooperative manner, the coordinate algorithm is needed. After UAVs reach the desired circle, we need to evenly space UAVs around the circle. In this manner, the localization error of the ground target could be reduced. The desired phase difference between adjoining UAVs could be $\theta_d = 2\pi / n$, where n denotes the number of UAVs. The phase between adjoining UAVs are $\theta_1, \theta_2, \theta_3$, and the phase difference $\triangle\theta$ could converge to zero by controlling the speed $s(t)$.

$$\triangle\theta = \theta_d - \theta_i \qquad i = 1, 2\cdots, n \tag{3}$$

An example of phase keeping with three UAVs is shown in Figure 2.

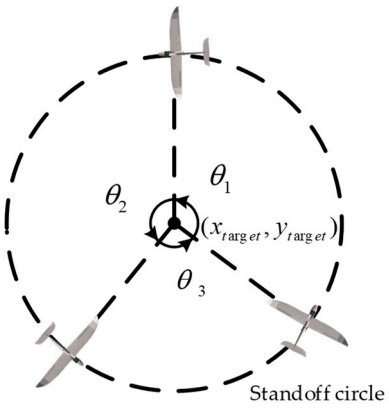

Figure 2. Scenario of phase keeping in standoff target tracking.

3. Lyapunov Vector Field Guidance Framework

Lyapunov vector field guidance proposed by Lawrence D [6] and its modified version are utilized to lead the fixed-wing UAV to approach the desired standoff distance and circle around a target in the local coordinate system. A nondimensional parameter is introduced to improve the convergence performance of LVFG [10]. The basic framework is

$$\begin{bmatrix} \dot{r} \\ r\dot{\theta} \end{bmatrix} = \frac{s}{\sqrt{r^4 + (c^2 - 2)r^2 r_d^2 + r_d^4}} \begin{bmatrix} -(r^2 - r^2{}_d) \\ c \cdot r \cdot r_d \end{bmatrix} \tag{4}$$

where c is a parameter, which can be used to adjust the speed of the generated field converging to the standoff circle. If $c = 2$, the vector field is the original version of LVFG.

In the above equation, $R = |\dot{r}|$ represents the speed of radial convergence to desired circle, and can be called a contraction component, while $T = |r\dot{\theta}|$ denotes circulation component, which denotes the tangent speed, as shown in Figure 3.

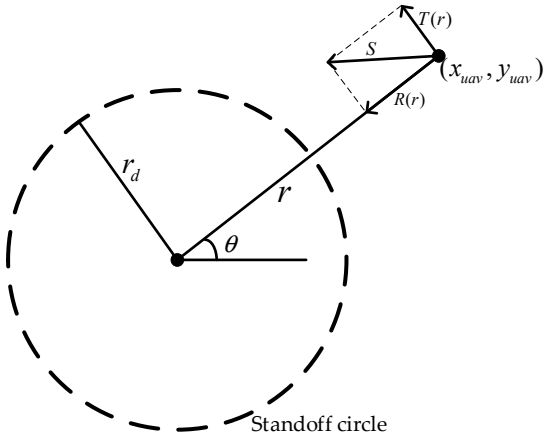

Figure 3. Construction component and circulation component.

To discuss the influence of c on the contraction and circulation, k can be represented as

$$k = \frac{r}{r_d} \tag{5}$$

Substituting Equation (5) into Equation (4), we get

$$R = \left| \frac{s(k^2 - 1)}{\sqrt{k^4 + (c^2 - 2)k^2 + 1}} \right| \tag{6}$$

$$T = \left| \frac{sck}{\sqrt{k^4 + (c^2 - 2)k^2 + 1}} \right| \tag{7}$$

Curves of contraction and circulation components with c as a constant are shown in Figure 4. Without loss of generality, we set s as a constant at 1.

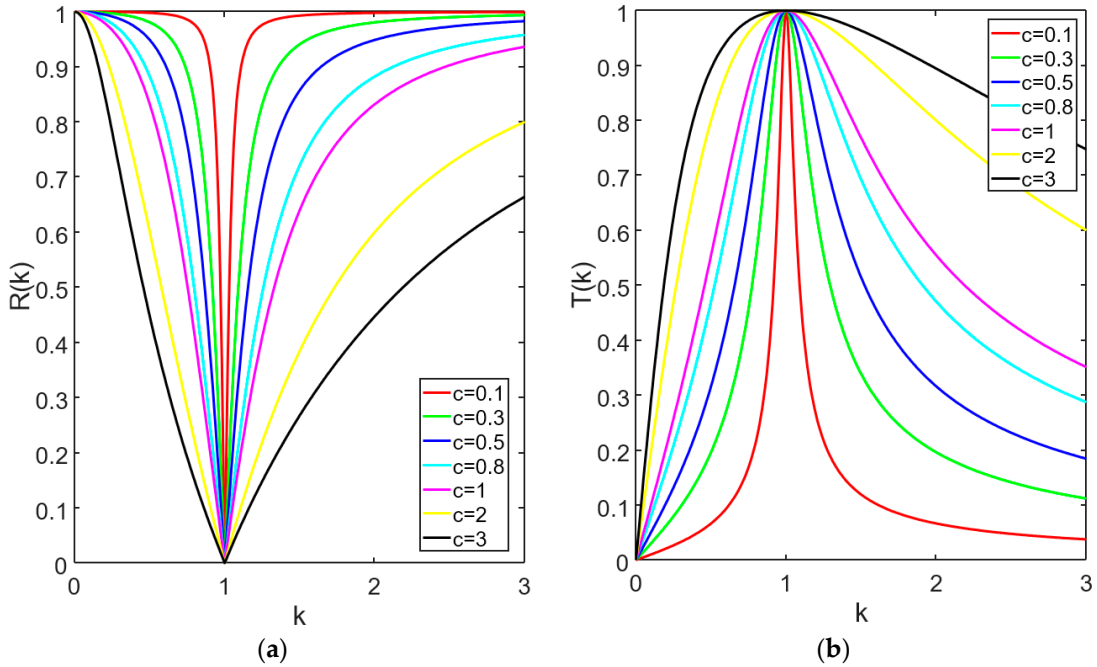

Figure 4. Curves of contraction and circulation components versus k in different c. (**a**) Curves of contraction component versus k; (**b**) Curves of circulation component versus k.

As shown in curves in Figure 4a, as k goes from $k=0$ or $k=\infty$ to $k=1$, meaning that the UAV approaches the standoff circle, the contraction component keeps decreasing, and the larger c is, the faster R goes down from 1, which means it spends more time converging to the desired circle. The opposite situation is shown in Figure 4b. The circulation component goes up more steeply as c is less when k is near $k=1$, which denotes that as c becomes smaller, the convergence speed in standoff tracking is improved significantly.

In the analysis of Shun Sun [12], when c becomes larger, the vector field converges slowly but can keep a distance from the prescribed radius stably; on the contrary, if c becomes smaller, the convergence time reduces sharply. However, in this situation, it is time-consuming on stabilization, where the UAV travels in and out of the loiter circle. Shun Sun copes with this problem by designing a series of guidance functions and searching for the optimal one before the UAV performs the mission. Obviously, offline search cannot adapt to the application scenario where the target is uncooperative with UAVs owing to the computing burden. In light of the above work, we will design a guidance function simultaneously taking into account both fast convergence and stable tracking performance in an online manner, which means we can adaptively balance the converging speed and stable tracking in real time.

Due to the maximum turning rate of the fixed-wing UAV, the curvature of the route must be analyzed. Transforming Equation (4) into a Cartesian coordinate system, the control manner of Lyapunov vector field guidance can be rewritten into Equation (8).

$$\begin{bmatrix} \dot{x} \\ \dot{y} \end{bmatrix} = -\frac{s}{r\sqrt{r^4+(c^2-2)r_d^2r^2+r_d^4}} \begin{bmatrix} (r^2-r_d^2)x_r + c\cdot r\cdot r_d\cdot y_r \\ (r^2-r_d^2)y_r - c\cdot r\cdot r_d\cdot x_r \end{bmatrix} \tag{8}$$

Then for a stationary target, the course can be represented as

$$\psi = a\tan(\frac{\dot{y}}{\dot{x}}) \tag{9}$$

Referring to work of Shun sun [12], we calculate the curvature by

$$\kappa = \frac{\dot{\psi}}{s} = \frac{s\cdot c\cdot r_d^3((c^2-2)r^2+2r_d^2) - \dot{c}\cdot r_d\cdot r(r^2-r_d^2)\sqrt{r^4+(c^2-2)r_d^2r^2+r_d^4}}{s(r^4+(c^2-2)r_d^2r^2+r_d^4)^{3/2}} \tag{10}$$

When c is a constant, Equation (10) reduces to

$$\kappa = \frac{\dot{\psi}}{s} = \frac{c\cdot r_d^3((c^2-2)r^2+2r_d^2)}{(r^4+(c^2-2)r_d^2r^2+r_d^4)^{3/2}} \tag{11}$$

It is worth noting that the traditional vector field is a special case where c is constant at 2, and the curvature of the classical vector field is always positive, as a monotone decreasing function of radical distance r, which means that it spends a long time on the path toward the loiter circle, resulting in an increase in convergence time. All curves intersect at the point $(rd, 1/rd)$, which implies that the vector field with different c converge to the standoff circle, and the UAV flies steadily along the circle.

Considering the maximum bank angle of the UAV, the maximum turning rate is limited, so the curvature is subject to a saturation constraint as

$$|\kappa| \le \frac{\dot{\psi}_{\max}}{s} \tag{12}$$

As shown in Figure 5, when c is small enough, an extremum lies on the curve near to the desired radius. This extremum may conflict with the curvature constraint of the UAV, which will be discussed in the subsequent section.

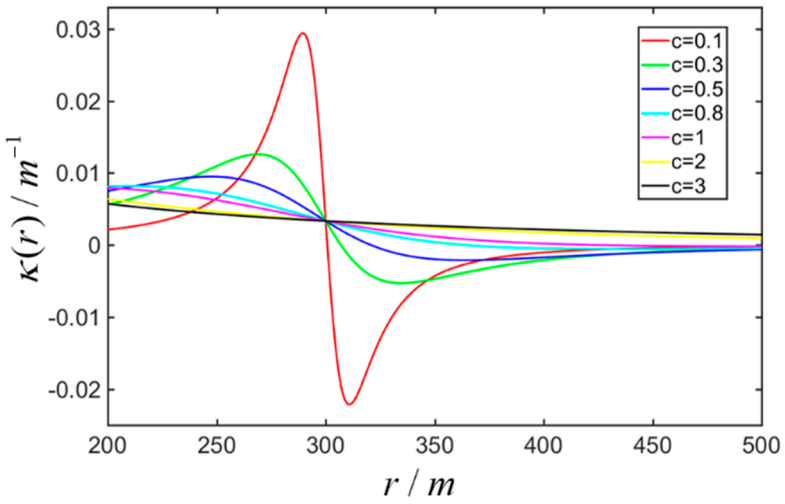

Figure 5. Vector field curvature κ versus r in different c ($rd = 300m$).

4. Design of Cooperative Tracking Guidance Laws

4.1. Design of Vector Field for Fast Convergence Target Tracking

When the UAV searches for the ground target, the target can be detected via an onboard camera when the UAV is far away from the target. Therefore, in this paper, we focus on the situation where the UAV is out of the standoff circle when it receives the 'tracking' command.

In the analysis in the previous section, smaller guidance parameter c makes the vector field more radial toward the desired circle. Although faster arrival at the standoff circle, it may result in greater time wasting on stabilization by making the aircraft repeatedly traverse the circle, as shown in Figure 6.

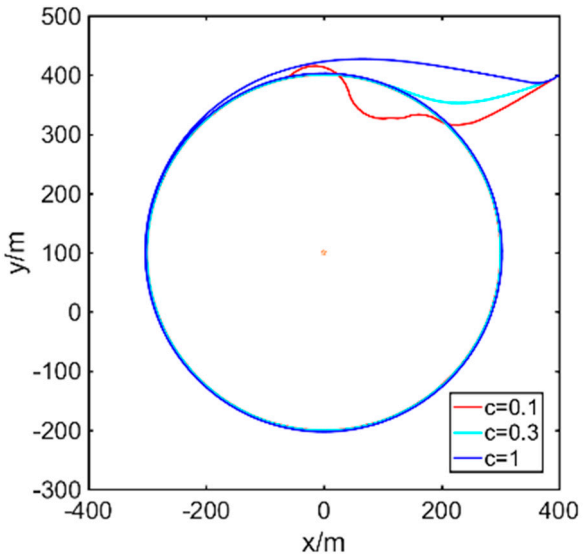

Figure 6. Trajectories with different guidance parameter c.

Two reasons may explain the event that trajectory intersects with the standoff circle. One reason is that the vector field will generate a non-flyable path for the aircraft with an inappropriate guidance parameter c. The other is that the starting position for the 'tracking mission' is too close to the standoff circle with the course pointing to the standoff circle.

As for the first reason, the extremum of the curvature near the standoff circle may exceed the curvature constraint of the UAV, despite the UAV turns at the maximum bank angle, and the trajectory intersects with the standoff circle, which leads to crossing over the circle several times.

Therefore, in order to reduce the convergence time, and put an end to crossing over the circle, the guidance parameter must be small enough but satisfies the curvature constraint.

The optimization problem can be expressed as:

$$\begin{cases} c = \arg\max\limits_{c}(\max(|\kappa(c,r)|) - \kappa_{\max}) \\ \quad s.t. \quad \max(|\kappa(c,r)|) < \kappa_{\max} \\ \quad where \quad r \in (r_d, +\infty) \end{cases}$$

It is too complex to calculate derivative of Equation (11) with respect to r, so an optimization algorithm based on the gradient descent method is developed to find $\max(|\kappa(c,r)|)$. In this way, the optimal guidance parameter can be obtained based on the search method below.

Algorithm: Optimal Guidance Parameter Search

Input: standoff radius r_d; maximum turning rate $\dot{\psi}_{\max}$; UAV cruising speed s; grid point of parameter $c_1, c_2, \cdots, c_m$;

Output: optimal parameter c_{opt};

Calculate the maximum curvature $\kappa_{\max}$ using Equation (11);

$d_{\min} = 10$;

$c_{opt} = 2$;

for $i = 1$ to m **do**

Obtain curvature function κ_{c_i} using Equation (11)

Find the extremum $|\kappa^{c_i}|_{\max}$ of the curvature function κ_{c_i} using the gradient descent method where $r \in (r_d, +\infty)$

if $|\kappa^{c_i}|_{\max} > \kappa_{\max}$ **then**

continue;

end if

$d = \kappa_{\max} - |\kappa^{c_i}|_{\max}$;

if $d < d_{\min}$ **then**

$c_{opt} = c_i$;

$d_{\min} = d$;

end if

end for

To cope with another problem, the inverse Lyapunov vector field (ILVF) is introduced. The ILVF is used to guide the UAV to fly away from the standoff circle. The ILVF can be obtained by changing the negative sign of $\dot{r}$ in Equation (4) to a positive one.

$$\begin{bmatrix} \dot{r} \\ r\dot{\theta} \end{bmatrix} = \frac{s}{\sqrt{r^4 + (c^2-2)r^2 r_d^2 + r_d^4}} \begin{bmatrix} r^2 - {r_d}^2 \\ c \cdot r \cdot r_d \end{bmatrix} \tag{13}$$

The control manner of ILVF can be rewritten into Equation (14) by transforming Equation (13) into a cartesian coordinate system

$$\begin{bmatrix} \dot{x} \\ \dot{y} \end{bmatrix} = \frac{s}{r\sqrt{r^4 + (c^2-2)r_d^2 r^2 + r_d^4}} \begin{bmatrix} (r^2 - r_d^2)x_r - c \cdot r \cdot r_d \cdot y_r \\ (r^2 - r_d^2)y_r + c \cdot r \cdot r_d \cdot x_r \end{bmatrix} \tag{14}$$

The Lyapunov vector field and inverse Lyapunov vector field can be shown intuitively in Figure 7. As shown in Figure 7, the vectors in the ILVF point away from the standoff circle.

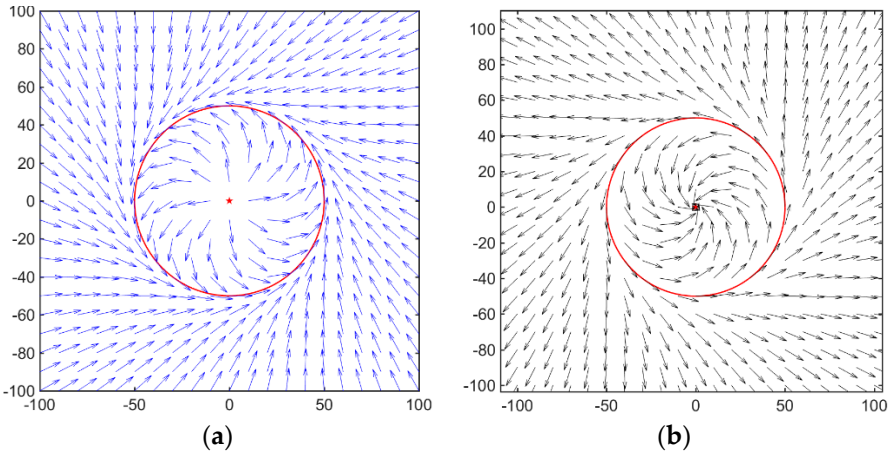

Figure 7. Lyapunov vector field and inverse Lyapunov vector field with $rd = 50m$ and $c = 0.7$. (**a**) Lyapunov vector field; (**b**) Inverse Lyapunov vector field.

When the start point for UAVs is too close for UAVs to avoid intersecting with the circle, the ILVF is enabled to guide UAVs to move away from the loiter circle.

By searching for the optimal guidance parameter c when UAV is far away from the standoff circle and fly away from the circle when it is too close, the proposed guidance law can guide UAV to converge to the standoff circle as fast as possible under the premise that the trajectory of the UAV does not cross the circle. In addition, the computation burden is lower than the method in reference [12], so that we can update the optimal guidance parameter in real time. In this way, we can adaptively balance the converging speed and stable tracking in real time.

4.2. Modification of the Guidance Law for Moving Targets Tracking

When a team of UAVs are tracking a ground moving target, the motion state of the target must be considered. As a correction item, the state of the target is used to modify the desired course of the UAV. If the UAV moves in the designed course in the local coordinate system of the target, the relationship between the modified velocity and target velocity is:

$$\begin{cases} v_g = v_t + \lambda v_d \\ v_{\min} \le |v_g| \le v_{\max} \end{cases} \tag{15}$$

where v_d is the desired velocity, $v_t = [v_x, v_y]^T$ is the velocity estimation of the target, v_g is the corrected desired speed in the global coordinate system, and λ is the correction factor.

Every UAV in the team could position the ground moving target using onboard sensors, while the result is not accurate enough for subsequent operations, such as guiding shells to strike or UAVs to track it stably. In this section, the state of the target is estimated based on the data fusion technology. A classic interactive multi-model is integrated with the unscented Kalman filter (IMM-UKF) to improve the geolocation precision. UKF is an improvement of EKF, which is important in integrating information [22]. Furthermore, a classic federated filter is adopted to reduce estimation errors by integrating independent sensor information from UAVs.

The framework of IMM-UKF with federated filter is shown in Figure 8. When tracking a moving target, every UAV localizes the target with a relatively low accuracy. The localization result will be processed using the IMM-UKF, which works well in estimating the state of the moving target. Then, the main filter collects the results of the local filter and distributes estimate results after time update and data fusion. The data fusion process with federated filter is introduced in Appendix A.

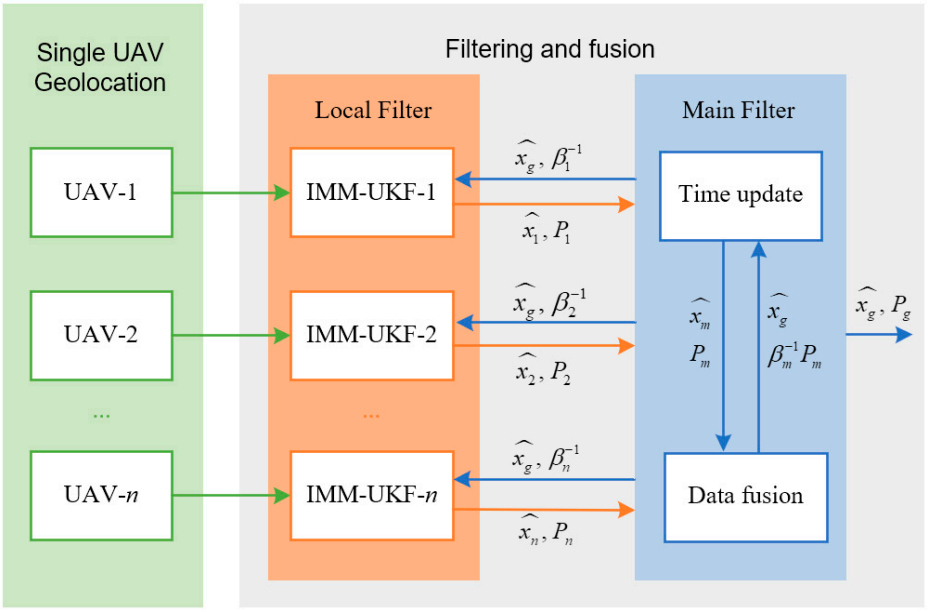

Figure 8. The framework of the state estimator.

In order to depict the state in a more accurate manner, three motion models are adopted in the IMM-UKF algorithm. Suppose state variables are

$$X = [x, v_x, y, v_y, a_x, a_y]^T$$

where x, y are the position variables, v_x, v_y are the velocity variables, a_x and a_y are the acceleration variables.

Motion models adopted in the paper will be introduced. The constant velocity model is used to model the target state in the constant velocity. All process noise mentioned below are zero-mean white Gaussian noise.

$$X_t[k+1] = A_{cv} X[k] + \omega_{cv}[k] \tag{16}$$

where

$$A_{cv} = \begin{bmatrix} 1 & T & 0 & 0 & 0 & 0 \\ 0 & 1 & 0 & 0 & 0 & 0 \\ 0 & 0 & 1 & T & 0 & 0 \\ 0 & 0 & 0 & 1 & 0 & 0 \\ 0 & 0 & 0 & 0 & 1 & 0 \\ 0 & 0 & 0 & 0 & 0 & 1 \end{bmatrix} \tag{17}$$

A_{cv} is the state transition matrix, and $\omega_{cv}[k]$ is the process noise.

The acceleration model can be expressed as

$$X_t[k+1] = A_{ca} X[k] + \omega_{ca}[k] \tag{18}$$

where

$$A_{ca} = \begin{bmatrix} 1 & T & 0 & 0 & T^2/2 & 0 \\ 0 & 1 & 0 & 0 & T & 0 \\ 0 & 0 & 1 & T & 0 & T^2/2 \\ 0 & 0 & 0 & 1 & 0 & T \\ 0 & 0 & 0 & 0 & 1 & 0 \\ 0 & 0 & 0 & 0 & 0 & 1 \end{bmatrix} \tag{19}$$

A_{ca} is the state transition matrix, and $\omega_{ca}[k]$ is the process noise.

Similarly, the turning model can be rewritten as

$$X_t[k+1] = A_s X[k] + \omega_s[k] \tag{20}$$

where

$$A_s = \begin{bmatrix} 1 & \frac{\sin(\omega T)}{\omega} & 0 & 0 & \frac{(1-\cos(\omega T))}{\omega^2} & 0 \\ 0 & \cos(\omega T) & 0 & 0 & \frac{\sin(\omega T)}{\omega} & 0 \\ 0 & 0 & 1 & \frac{\sin(\omega T)}{\omega} & 0 & \frac{(1-\cos(\omega T))}{\omega^2} \\ 0 & 0 & 0 & \cos(\omega T) & 0 & \frac{\sin(\omega T)}{\omega} \\ 0 & -\omega\sin(\omega T) & 0 & 0 & \cos(\omega T) & 0 \\ 0 & 0 & 0 & -\omega\sin(\omega T) & 0 & \cos(\omega T) \end{bmatrix} \tag{21}$$

A_s is the state transition matrix, and $\omega_s[k]$ is the process noise.

The estimation process is introduced in Appendix B. After the state estimation, we get the estimation of the current state

The position vector $[x, y]^T$ is used for the basic tracking of the static target while the velocity vector $v_t = [v_x, v_y]^T$ is utilized to modify the guidance law of UAVs when tracking a moving target.

4.3. Phase Keeping for Cooperative Tracking

Besides standoff tracking of a ground target, it is of vital importance to control the intervehicle phase. On the one hand, the unpredicted maneuver of a vehicle can be observed when UAVs are distributed evenly on the circle. On the other hand, the precision of target localization can be enhanced by fusing independent sensor information.

We develop a new controller based on the speed controller from Frew E W [7], which can achieve faster convergence. Different from the original method, we set an ideal seat for each UAV. These ideal seats are evenly spaced around the circle. Then, the speed controller is utilized to guide each UAV to its ideal seat by controlling the speed. As a result, the team of UAVs will be evenly distributed on the circle. Without loss of generality, we adopt three UAVs to perform the tracking mission, and UAV1, UAV2, and UAV3 are arranged counterclockwise, as shown in Figure 9.

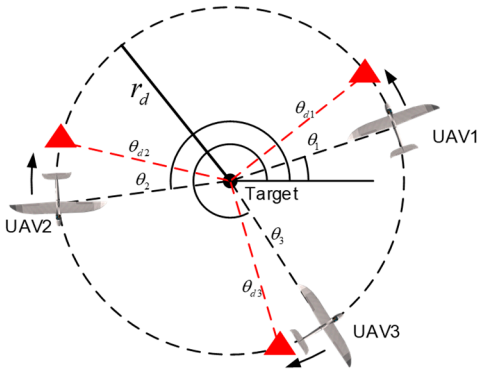

Figure 9. Cooperative target tracking using three unmanned aerial vehicles (UAVs).

Figure 9 shows a team of three-UAVs, with corresponding phase angles θ_1, θ_2, and θ_3 defined relative to the instantaneous tracking circle. Consider a phasing Lyapunov function

$$V_p = \sum_{i=1}^{3} (\Delta\theta_i)^2 \tag{22}$$

where $\Delta\theta_i = \theta_{di} - \theta_i \quad i = 1,2,3$ denotes the unwrapped difference between the phase angle and the desired angle. The method for calculating the desired angle will be introduced later. The time derivation of this function is

$$\frac{dV_p}{dt} = 2\sum_{i=1}^{3} \Delta\theta_i \bullet (\dot{\theta}_{di} - \dot{\theta}_i) \tag{23}$$

Then, we choose the angular speed commands

$$\dot{\theta}_i = k(\frac{r_d}{r_i})^2(\theta_{di} - \theta_i) + \frac{v_{uav}}{r_d} \quad i = 1,2,3 \tag{24}$$

where k is a positive proportional gain. Since the desired seat circles around the UAV cruising at v_{uav}, the desired angle speed is

$$\dot{\theta}_{di} = \frac{v_{uav}}{r_d} \quad i = 1,2,3 \tag{25}$$

Then, Equation (24) results in

$$\frac{dV_p}{dt} = -2k(\frac{r_d}{r})^2 \sum_{i=1}^{3} (\theta_{di} - \theta_i)^2 = -2k(\frac{r_d}{r})^2 V_p \tag{26}$$

Note that $\dot{V}_p$ is negative semi-definite, which ensures that V_p converges exponentially to zero, hence the relative angle $\Delta\theta_i = \theta_{di} - \theta_i \quad i = 1,2,3$ converges exponentially to zero, which means the UAV phase angle converges to the desired angle.

The corresponding speed control commands are then

$$v_{di} = k(\frac{r_d}{r_i})^2(\theta_{di} - \theta_i)r_d + v_{uav} \quad i = 1,2,3 \tag{27}$$

The term $(r_d/r_i)^2$ is introduced to restrain the phase keeping operation when the UAVs are far away from the target [7].

In the above algorithm, the choice of the desired seat is of vital importance. The optimal choice of the desired seats allow UAVs to reduce their speed, as well as the burden on the flight controller. As shown in Figure 9, the total angle difference between the desired seat and the corresponding UAV is

$$D_p = |\theta_{d1} - \theta_1| + |\theta_{d2} - \theta_2| + |\theta_{d3} - \theta_3| \tag{28}$$

where $\theta_{d2} = \theta_{d1} + 2\pi/3$, $\theta_{d3} = \theta_{d1} + 4\pi/3$. When $\theta_{d1} = (\theta_1 + \theta_2 + \theta_3 - 2\pi)/3$, D_p reaches the minimize value. Thus, the desired phase for each UAV in any instantaneous frame can be calculated.

5. Experiments and Results

5.1. Numerical Simulation

To illustrate the performance of the guidance laws based on the proposed algorithm, a series of tests in numerical simulation are conducted, and extensive comparison and analysis are performed. In the first step, the experiments on tracking stationary targets are carried out, then for tracking moving targets, target state estimations are conducted. At last, cooperative tracking simulation

verifies the faster convergence of the proposed controller. In numerical simulations, base configurations are listed in Table 1.

Table 1. Key parameters in the numerical simulation.

Parameter	Description	Value
R	standoff distance	$300m$
s	cruising speed of UAVs	$20m/s$
$s_{\min}$	minimum speed of UAVs	$13m/s$
$s_{\max}$	maximum speed of UAVs	$25m/s$
$a_{\min}$	minimum acceleration of UAVs	$-2m/s^2$
$a_{\max}$	maximum acceleration of UAVs	$2m/s^2$
$\dot{\psi}_{\max}$	maximum course rate	$0.2rad/s$

5.1.1. Standoff Tracking of Stationary Targets

The numerical simulation of standoff tracking of the stationary target is carried out to verify the superiority of the proposed algorithm over other guidance laws. Stable tracking of stationary targets is the base of tracking moving targets and cooperative tracking.

In this paper, methods proposed by Shun Sun [12] and Frew [7] are compared with our guidance laws in the same simulation configuration. Two simulations are carried out with different initial UAV position. In simulation A, the initial position of the UAV is far away from the standoff circle, while in simulation B, it is near the standoff circle. Supposing UAV state vectors are $[x, y, \psi, v]^T$, where x, y are the coordinates of the UAV position, ψ is the current heading angle, and v is the UAV speed.

In Simulation A, the initial state vector of the UAV is $[600, 600, 1.25\pi, 18]^T$. As shown in Figure 10a, obviously, the proposed guidance law guides the UAV faster to the standoff circle. The UAV guided by the proposed guidance law settles to the standoff circle at $t = 53s$, while ShunSun's method at $t = 112s$ and Frew's method at $t = 210s$ in Figure 10b. Reasons can be found by analyzing Figure 10c: The proposed guidance law guides the UAV to fly at a bigger course rate when approaching the standoff circle, resulting in faster settling to the desired distance. In contrast, the other two methods guide the UAV in a relatively gentle manner. UAVs fly at a smaller course rate, squandering time on the path to the standoff circle.

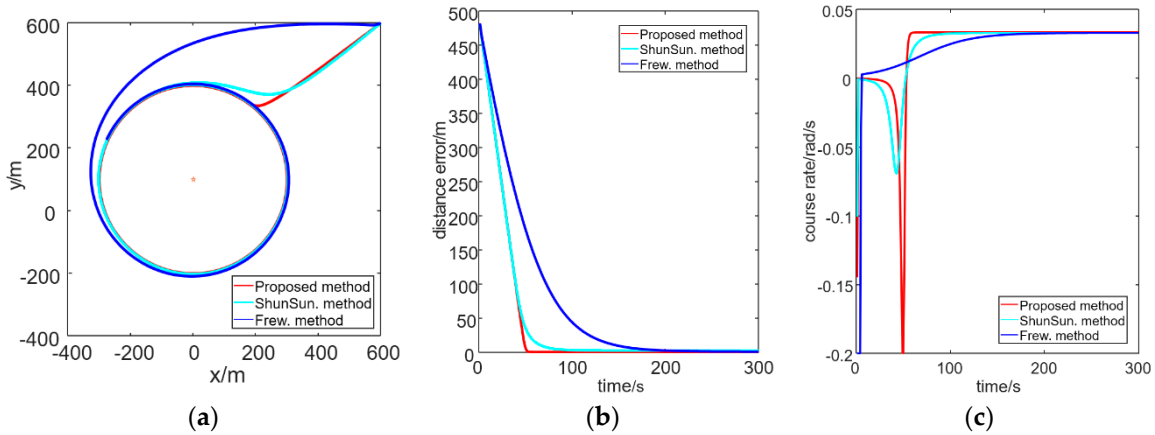

Figure 10. Experiments results with respect to an initial UAV position far away from the standoff circle. (**a**) Trajectories of UAVs; (**b**) Distance error versus time; (**c**) Course rate versus time.

In simulation B, the initial UAV state vector is $[300, 300, 1.5\pi, 18]^T$, which is close to the standoff circle. The trajectories are shown in Figure 11a. When the initial position of the UAV is near the standoff circle, the trajectory will intersect with the circle if the UAV obeys the guidance generated

by the normal Lyapunov vector field. The distance error curvatures of this situation are denoted as the cyan line and blue line in Figure 11b, where the values of the interval $(10, 110)$ are negative. In this situation, the proposed guidance law guides the UAV to fly away from the standoff circle temporarily using the inverse Lyapunov vector field and go back when the UAV is able to converge to the standoff circle without intersecting with the standoff circle, whose distance error curvature is denoted as the red line in Figure 11b. The red line corresponding to the proposed method has no negative distance error, which means that the UAV trajectory does not intersect with the standoff circle. As a side effect, the UAV flies at the maximum turning rate before settling to the standoff circle, as shown in Figure 11c.

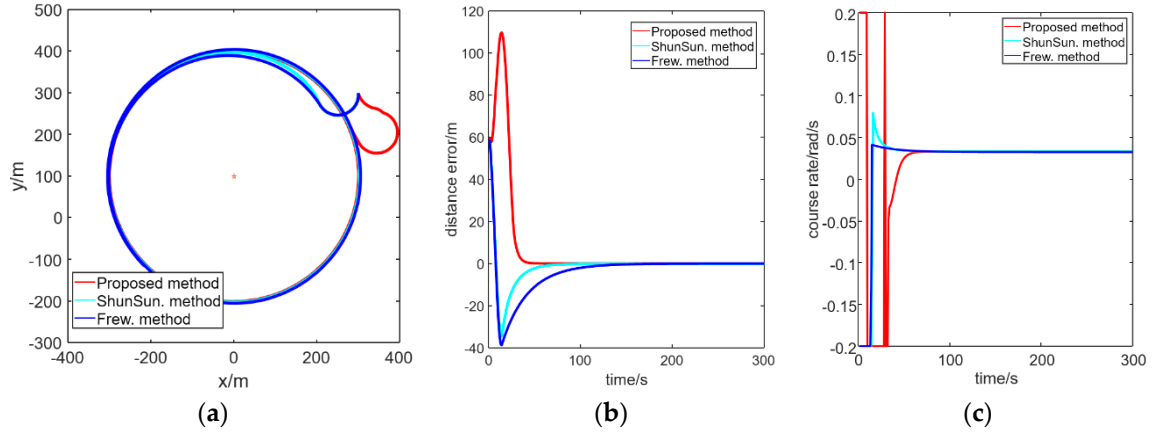

Figure 11. Experiments results with respect to an initial UAV position near the standoff circle. (**a**) Trajectories of UAVs; (**b**) Distance error versus time; (**c**) Course rate versus time.

In this experiment, the guidance law generated by our algorithm is adopted to guide the UAV when it is at different distances from the desired circle. When the UAV is far away from the standoff circle, the trajectory converges to the circle faster than the compared algorithm and circles around the target stably without intersecting with the desired circle. When the UAV is close to the circle, our algorithm guides the UAV to fly away from the circle temporarily. In this way, the trajectory will not intersect with the circle.

5.1.2. Estimation of Target States Using IMM-UKF

In this section, numerical experiment is carried out to verify the validity of the state estimator. When estimating the target state using IMM-UKF, the motion models mentioned in Section 4 are used. The target trajectory is designed as shown in Figure 12. A gaussian noise of which $\mu = 0$ and variance $\sigma^2 = 10$ is imposed on the position of the target in the direction x and y, respectively.

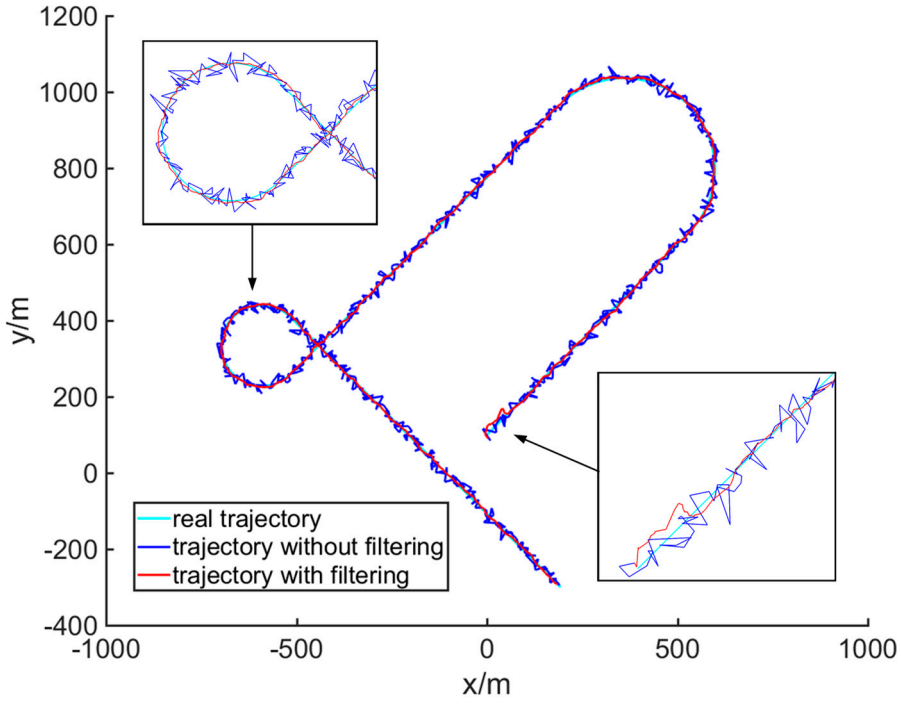

Figure 12. Trajectory and position estimation of the moving target.

The estimation error in position is shown in Figure 13. Based on the IMM-UKF state estimation algorithm, the position error is reduced from 10.4 m to 5.35 m. It can be seen that when the target is turning around $t \in (180,280) \bigcup (500,600)$, the error is relatively significant, owing to the fact that the motion model is not accurate enough.

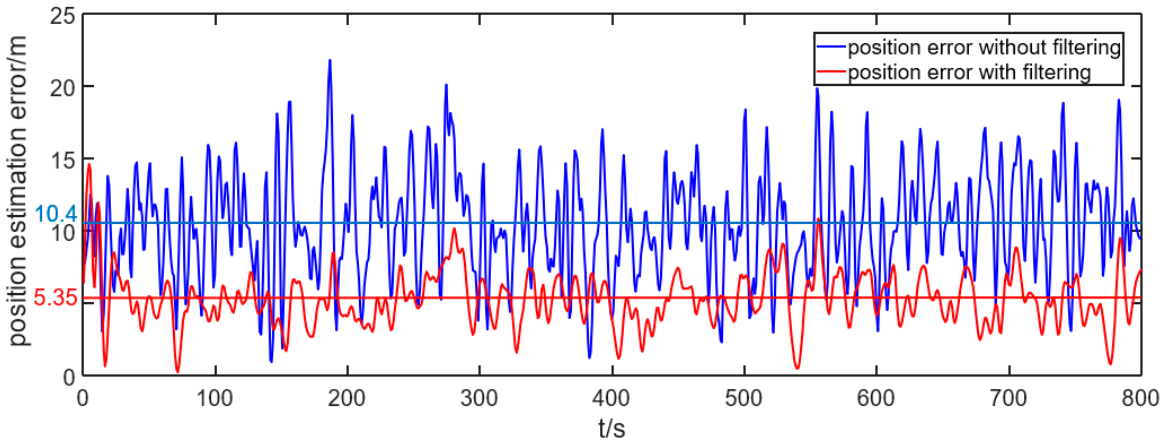

Figure 13. Position estimation error versus time.

The same trend can be seen in the velocity estimation (Figure 14a,b), where $t \in (180,280) \bigcup (500,600)$, the velocity estimation is relatively inaccurate.

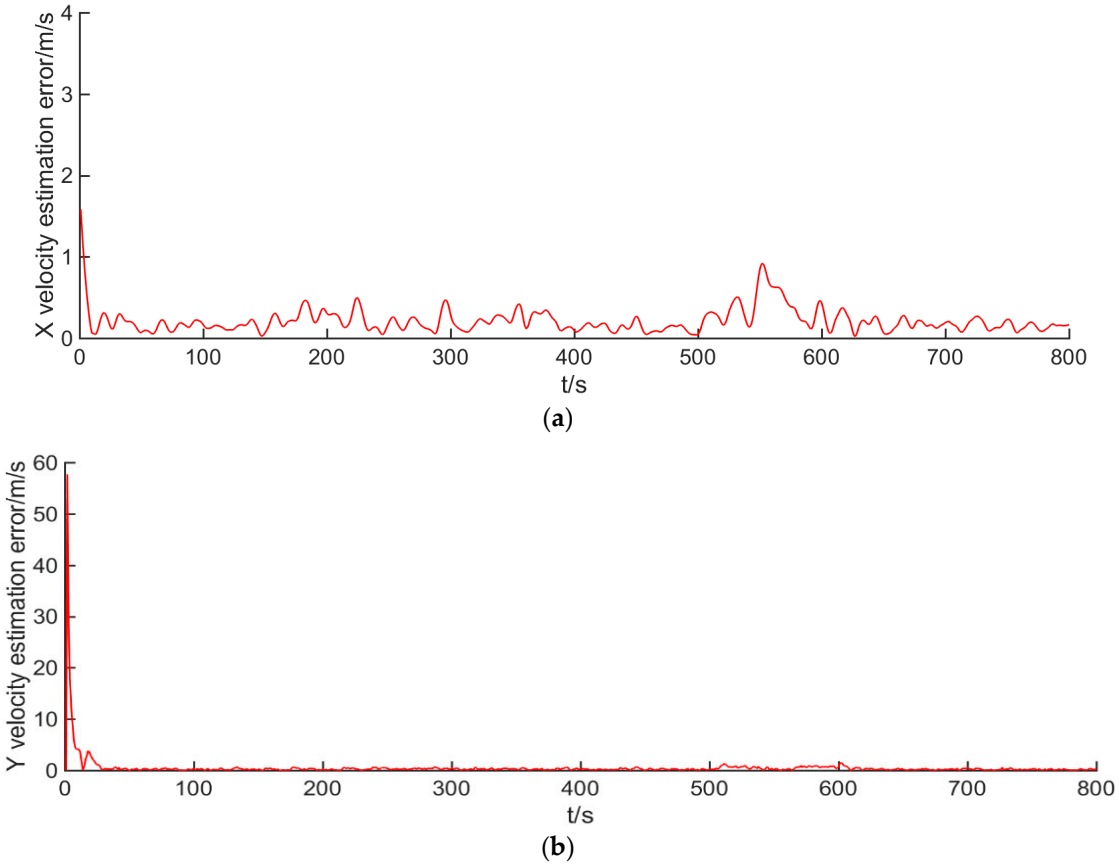

Figure 14. Velocity estimation results. (**a**) X velocity estimation error versus time; (**b**) Y velocity estimation error versus time.

This section presents the experimental results of target state estimation. The estimator works well when the target moves along a straight line, while the estimation error increases when the target changes its moving direction. The results are consistent with the notion that it is harder to estimate the state of nonlinear motion.

5.1.3. Phase-Keeping in Cooperative Standoff Tracking

In order to demonstrate the performance of the phase keeping algorithm, a team of three UAVs maintain the same desired distance, circumnavigating around a stationary target. The cruising speed of the UAV is $20m/s$, its flight speed is restricted within $13m/s \le v_{uav} \le 25m/s$, and the acceleration constraint is $-2m/s^2 \le a_{uav} \le 2m/s^2$. The desired standoff distance is $400m$.

Figure 15a shows three UAVs approaching the loiter circle. We utilized the standoff tracking algorithm presented above with the same parameter on the proposed phase keeping method and the method proposed by Frew etc. [7]. It is obvious that three UAVs stick to the desired circle and maintain the desired standoff distance. Figure 15b,c shows the velocity of vehicles and phase differences between adjoining UAVs versus time. Compared with the reference method, the proposed algorithm settles down to the cruising speed faster, and the velocity does not change back and forth. The phase difference can converge to the desired value in a shorter time.

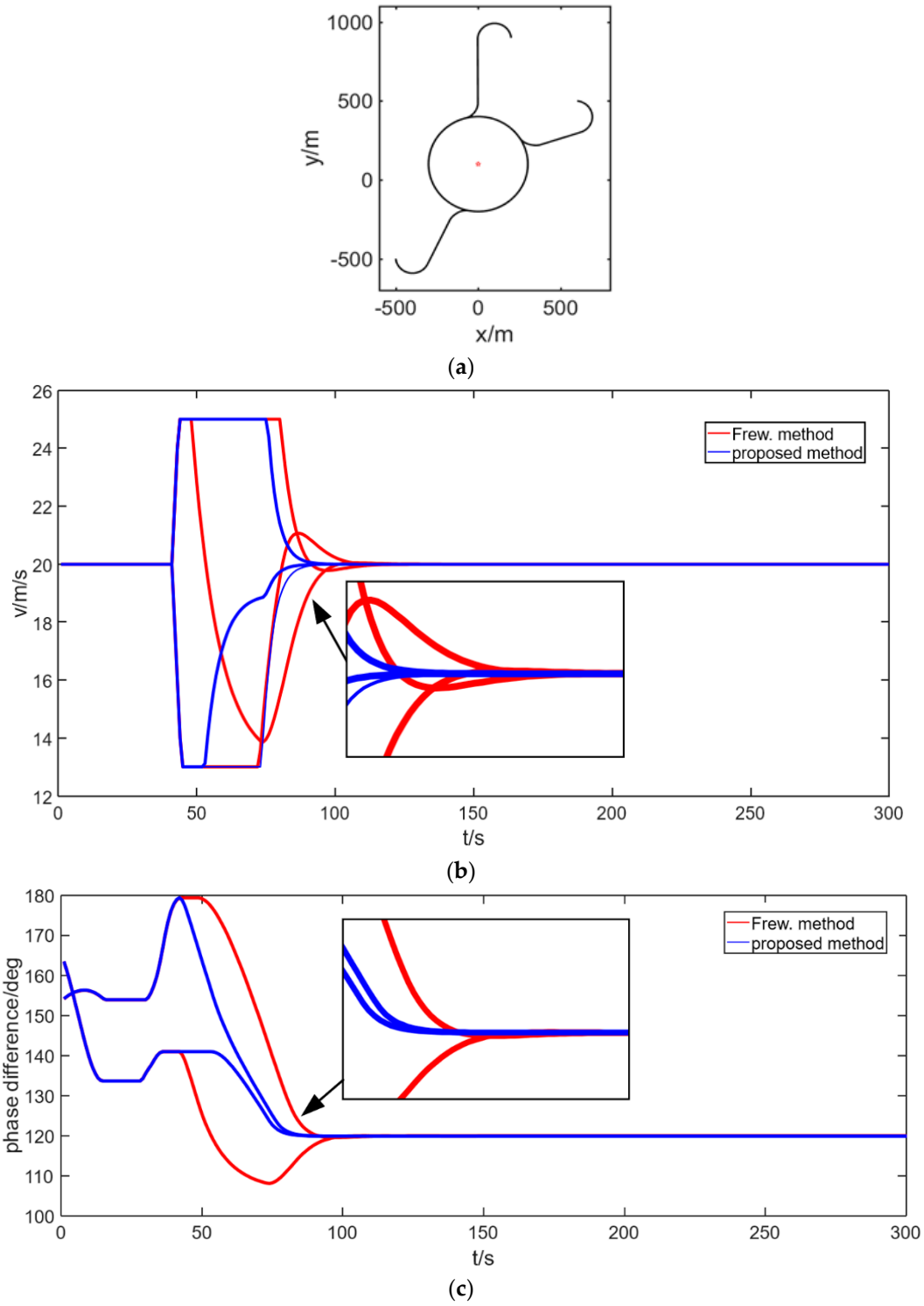

Figure 15. Experiments results of phase keeping. (**a**) Trajectories of three UAVs; (**b**) Curves of velocity versus time; (**c**) Curves of phase difference versus time.

From the experiment results, we can conclude that whether in velocity or in phase difference, the proposed controller shows shorter stabilization time and less overshot.

5.2. Hardware-In-the-Loop Simulation

In the above numerical simulation, the fixed-wing UAV is treated as a mass point, the flight constraints, such as the minimum turning angle and performance of the FCS, have not been

considered. Therefore, we transfer the proposed algorithm to the HIL simulation on tracking ground targets in different motion states to verify the feasibility in high-fidelity experiments.

5.2.1. HIL Simulation Setup

In this paper, we further use a HIL simulation platform to validate the proposed algorithm. The HIL simulation system consists of a X-Plane10 Flight Simulator, Pixhawk4 autopilots, and an onboard computer for each UAV, and a ground control station called Superstation. The simulation platform is shown in Figure 16. There are three simulation UAVs (UAV1, UAV2, UAV3) connected to the ground control station via serial ports, and the detailed components of simulation for UAVs are placed on the right of Figure 16. The laptops and onboard computer used in the HIL simulation are shown in Figure 17.

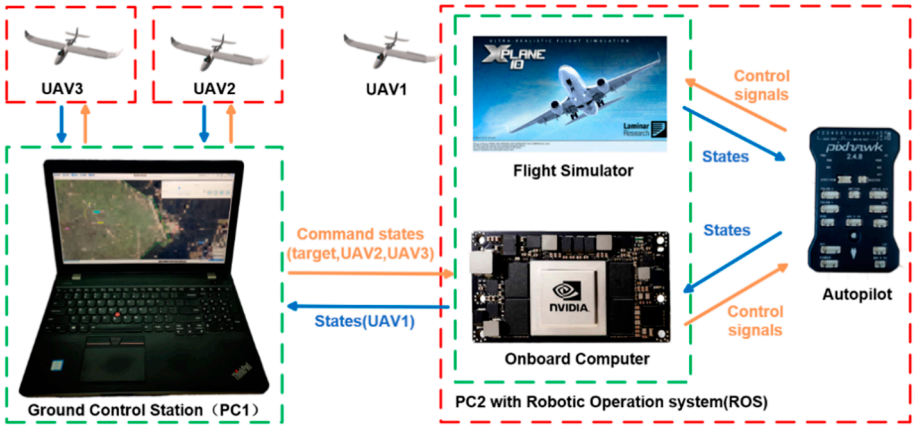

Figure 16. The architecture of the HIL simulation. The left part shows the Ground Control Station, and the right part places the detailed components (flight simulator, autopilot, and onboard computer) and the information flow among them. The modules are operated or connected in the robot operation system (ROS).

Figure 17. The laptops and onboard computer used in the HIL simulation. The ground control station is in the upper right corner, and other laptops are simulations for UAVs.

The high-fidelity aircraft simulation software X-plane 10 is a comprehensive and powerful flight simulator for the personal computer, which is often used in HIL simulation [23,24]. We choose the HILStar 17F aircraft as the controlled object. Pixhawk 4 autopilot controls the UAV to fly along the commands. The onboard computer receives the states of the target and other UAVs and sends control policies generated by the proposed algorithm to Pixhawk 4. The ground control station monitors the states of the target and all UAVs, which are distributed to each UAV, and can control multiple UAVs by switch control modes.

Figure 18 displays a snapshot of the target standoff tracking, and Figure 18a shows the controlled objective used in the HIL simulation, which is rolling right, indicating that the UAV is circling

clockwise. Figure18b displays the cooperative tracking of a moving target using three UAVs, all of which are circling clockwise.

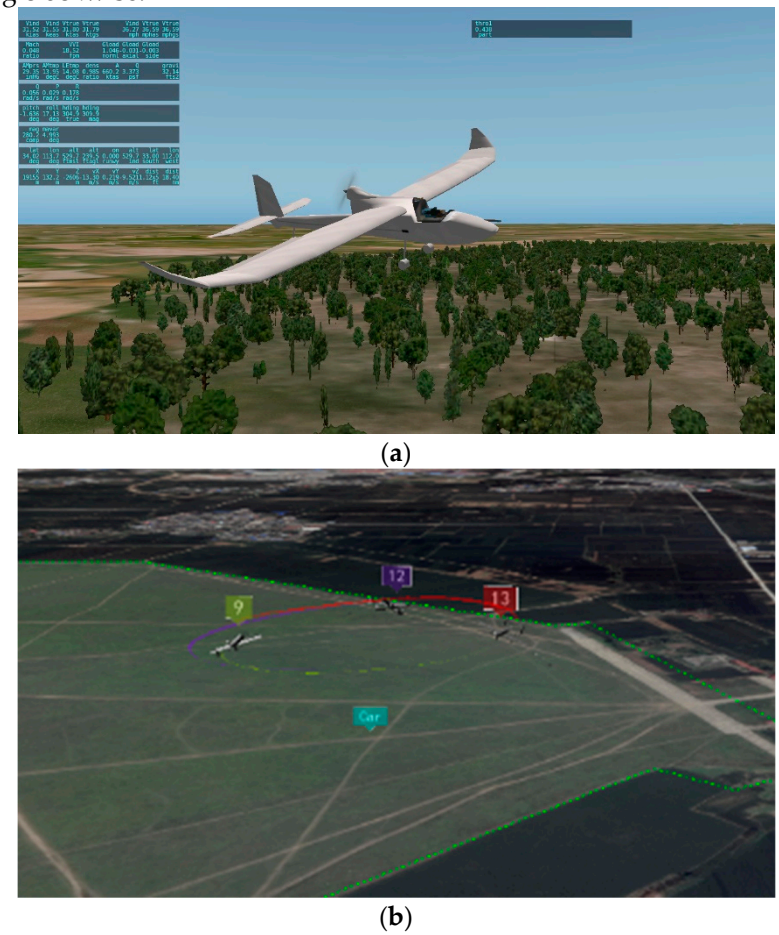

(**a**)

(**b**)

Figure 18. The snapshots of the target standoff experiments in HIL simulation in different perspectives. (**a**) HILStar 17F used in the X-plane simulator, (**b**) The tracking trajectory of the UAV around the car.

The detailed implementation process can be:

(1) The ground control station distributes three sets of pre-processed data obtained by onboard sensors to three UAVs;
(2) The onboard computer estimates the state of the target using pre-process data received from the ground control station via the IMM-UKF and federated filter;
(3) The onboard computer generates the desired course angle, modifies it with the predicted velocity vector, adjusts the desired speed if the phase difference needs to be adjusted, and sends the desired course and speed to the autopilot;
(4) The autopilot sends control commands to the flight simulator, receives aircraft status, and forwards it to the onboard computer.

As shown in Figure 19, the simulation environment is designed as follows: As soon as the fixed-wing UAVs takes off from the runway, they hover over the standby point until receiving the "tracking" command. Then, they track the ground moving target under the command generated by the tracking algorithm. The moving target moves from start point A, and finally stops at the end point D, passing the turning points B and C. The target moves at a relatively high speed v_{th} from A to B, and a relatively low speed v_{tl} from B to C. After a sharp turn on the right at C, the target moves at a constant acceleration at a_t and stops at D.

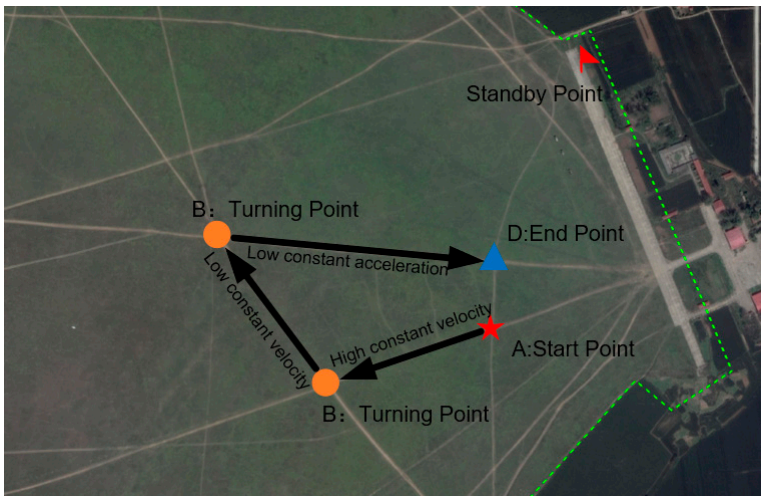

Figure 19. The target trajectories and moving speed in the simulation environment.

All key parameters in the HIL simulation are listed in Table 2.

Table 2. Key parameters in the HIL simulation.

Parameters	Description	Value
R	standoff distance	$90m$
s	cruising speed of the UAV	$14m/s$
$s_{\min}$	minimum speed of the UAV	$10m/s$
$s_{\max}$	maximum speed of the UAV	$18m/s$
$a_{\min}$	minimum acceleration of the UAV	$-2m/s^2$
$a_{\max}$	maximum acceleration of the UAV	$2m/s^2$
$\dot{\psi}_{\max}$	maximum course rate	$0.2rad/s$
v_{tl}	low constant speed of the target	$3m/s$
v_{th}	high constant speed of the target	$7m/s$
a_t	constant acceleration of the target	$1.5m/s^2$

For simplicity, several stages are defined in this paper. When UAVs fly from the standby point to the start point, we call it the 'gathering' stage, and UAVs adjust the phase difference over the start point A during the 'adjusting' stage. Similarly, the periods from start point A to turning point B, from turning point B to turning point C, and from turning point B to end point D correspond to the 'high-speed' stage, 'low-speed' stage, and 'accelerating' stage, respectively.

5.2.2. HIL Simulation Results

As shown in Figure 20, three UAVs cooperatively track the target moving on ground of which the trajectories are described in Figure 19. In Figure 20a, UAVs clump around the start point after receiving "tracking" command at the standby point. UAVs are distributed evenly around the standoff circle by adjusting speed in Figure 20b. Figure 20c illustrates the cooperative tracking of the target moving at a constant velocity, while the trajectories of UAVs tracking accelerating targets are shown in Figure 20d. We can intuitively see that the team of three UAVs can cooperatively track the target moving on ground, distributed in a circle with a suitable angular difference.

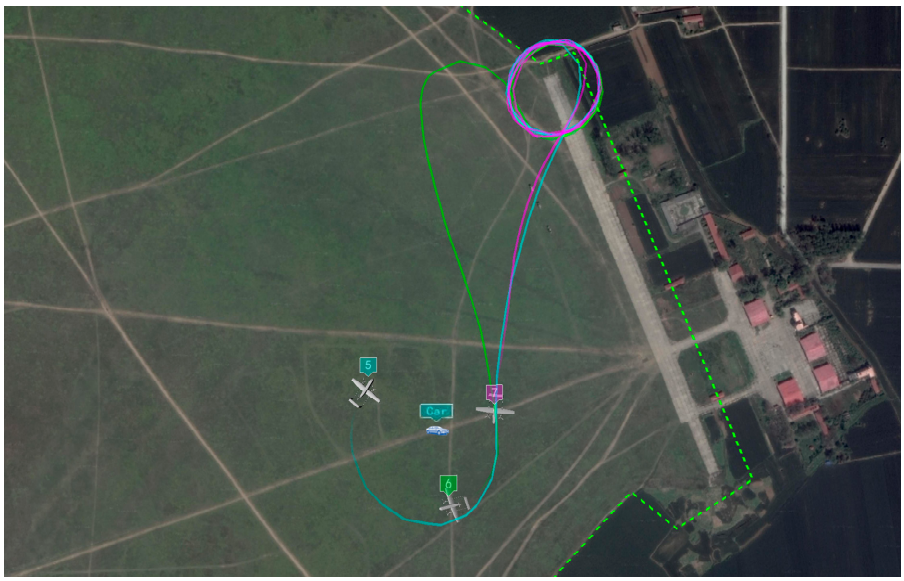

(**a**)

(**b**)

(**c**)

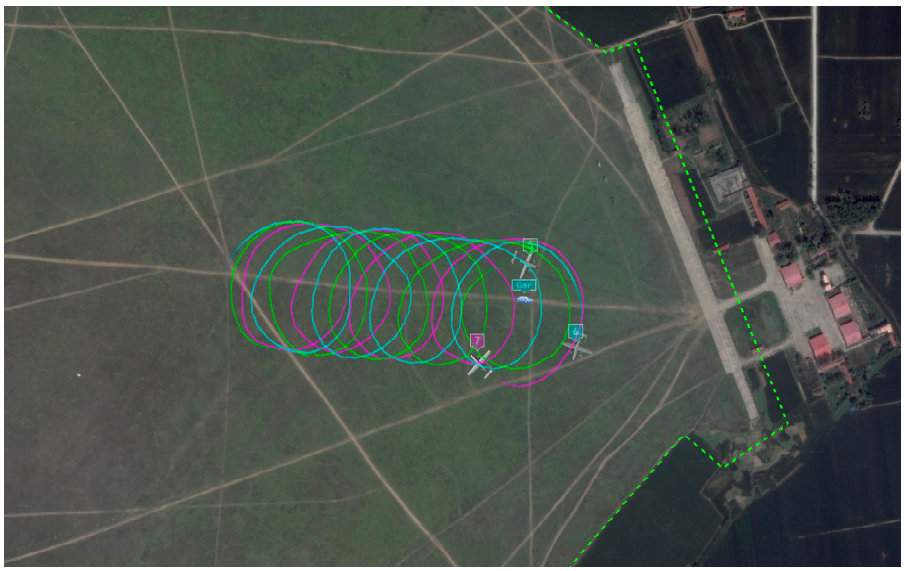

(**d**)

Figure 20. The snapshots of cooperative standoff tracking shown on the Ground Control Station in the HIL simulation. (**a**) Gather around the target; (**b**) Adjust phase difference; (**c**) Track the constant-speed target; (**d**) Track the accelerating target.

The details of tracking performance are listed in Figures 21 and 22. In the 'gathering' stage shown in Figures 21a and 22a, the distance error deceases rapidly to zero as UAVs fly toward the start point at the maximum speed. In the early stage, such as interval (I) in Figures 21a and 22a, UAVs hover over the standby point, which is far away from the start point, so the phase difference relative to the target undergoes drastic changes.

In the phase adjusting stage, UAVs mainly adjust the phase difference between neighboring UAVs. In interval (II) as shown in Figure 21b, the distance errors of three UAVs gradually converge to zero, but there is a slight shock around zero in interval (III), owing to the unstable UAV model in the Xplane simulator. In interval (II) as shown in Figure 22b, the phase difference converges to the desired phase (120^{o}) while the UAVs speed varies, which is controlled by the policies generated by Equation (28). In interval (III) as shown in Figure 22b, the phase difference between neighboring UAVs is stably near the desired value.

When the ground target is moving, the tracking performance is closely related to the target speed. Tracking the low-speed targets is relatively easier than tracking high-speed and accelerating targets, and tracking the accelerating target is the hardest task, which is obviously shown in the distance error fluctuation (Figure 21c–e). The main reason may be that the estimation of the state of low-speed targets is relatively easier, while for accelerating targets, the estimation is the most inaccurate. Furthermore, the estimation results are utilized to modify the guidance laws, so tracking performance is impacted. Correspondingly, the phase difference error shows a similar trend (Figure 22c–e) as distance error, which complies with the fact that performance in distance keeping influences phase keeping a great deal.

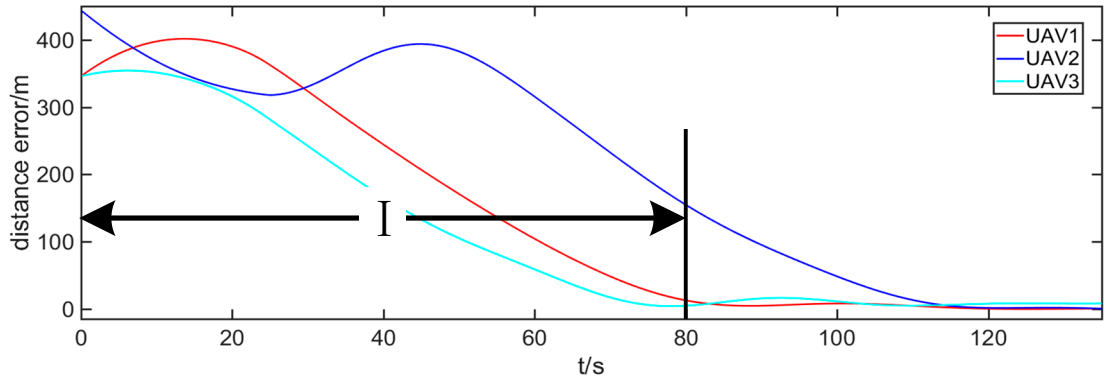
UAV1
UAV2
UAV3
distance error/m
t/s
I

(**a**)

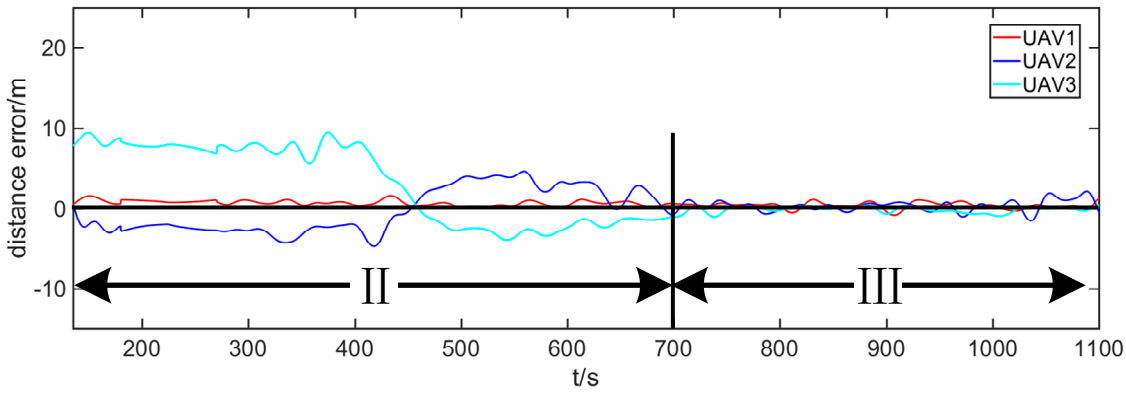
UAV1
UAV2
UAV3
distance error/m
t/s
II
III

(**b**)

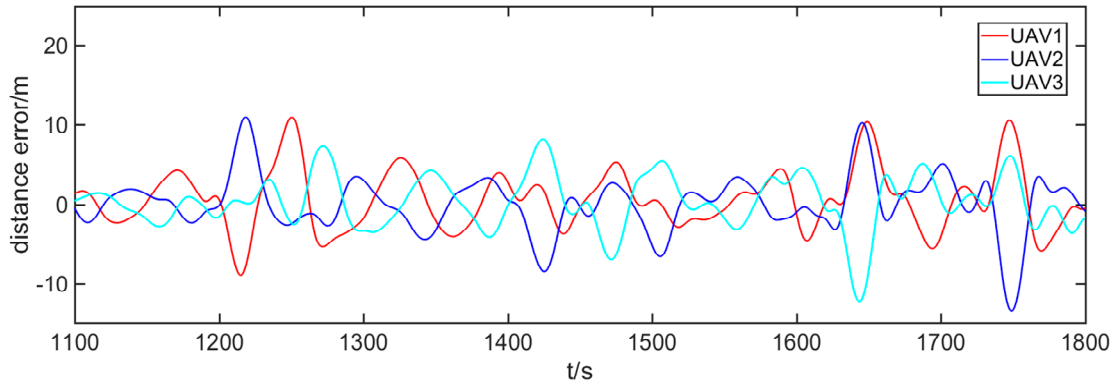
UAV1
UAV2
UAV3
distance error/m
t/s

(**c**)

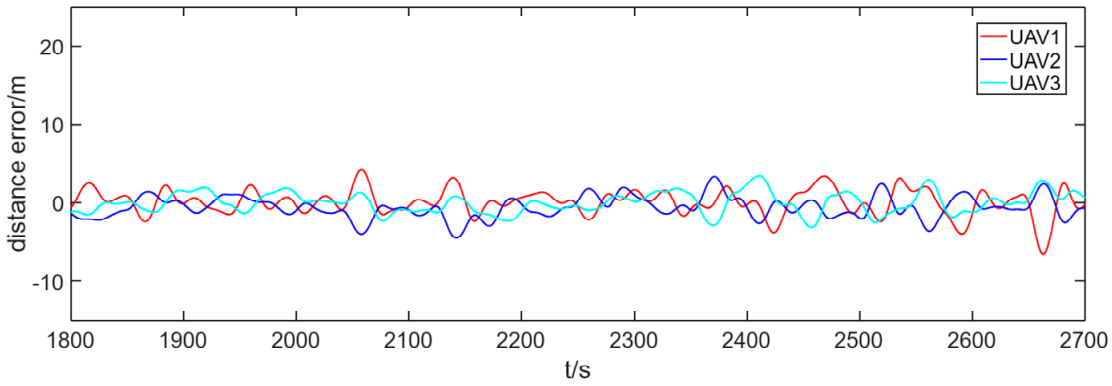
UAV1
UAV2
UAV3
distance error/m
t/s

(**d**)

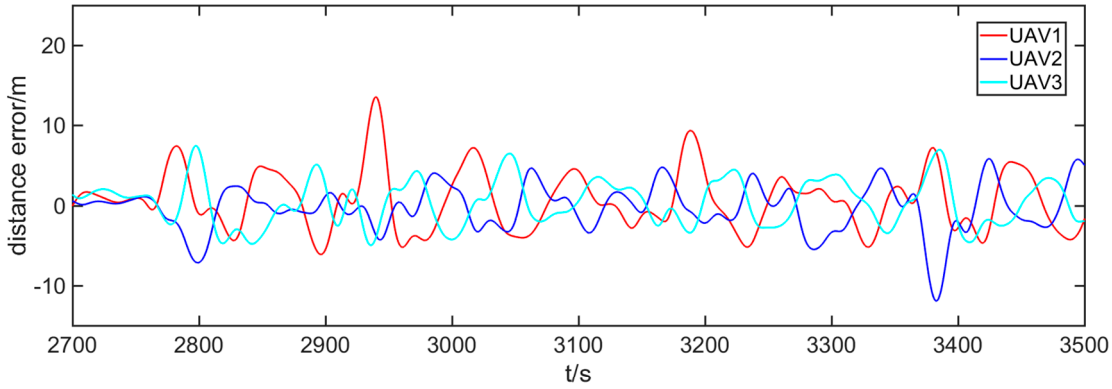

(**e**)

Figure 21. The standoff tracking distance error. (**a**) Distance error in the "gather" stage; (**b**) Distance error in the "phase adjusting" stage; (**c**) Distance error in the "high-speed" stage; (**d**) Distance error in the "low-speed" stage; (**e**) Distance error in the "accelerating" stage.

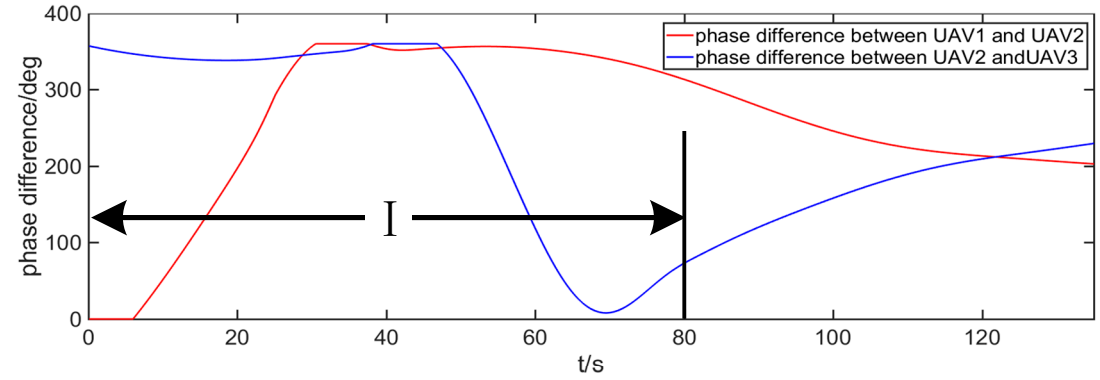

(**a**)

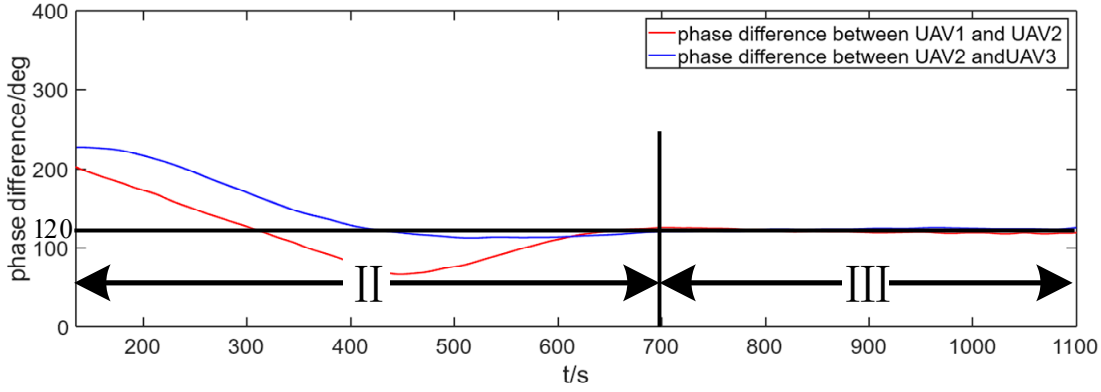

(**b**)

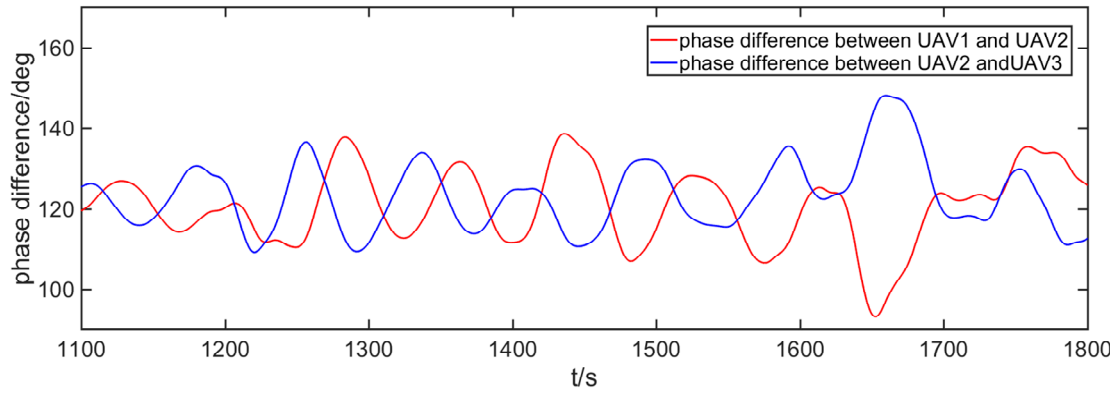

(**c**)

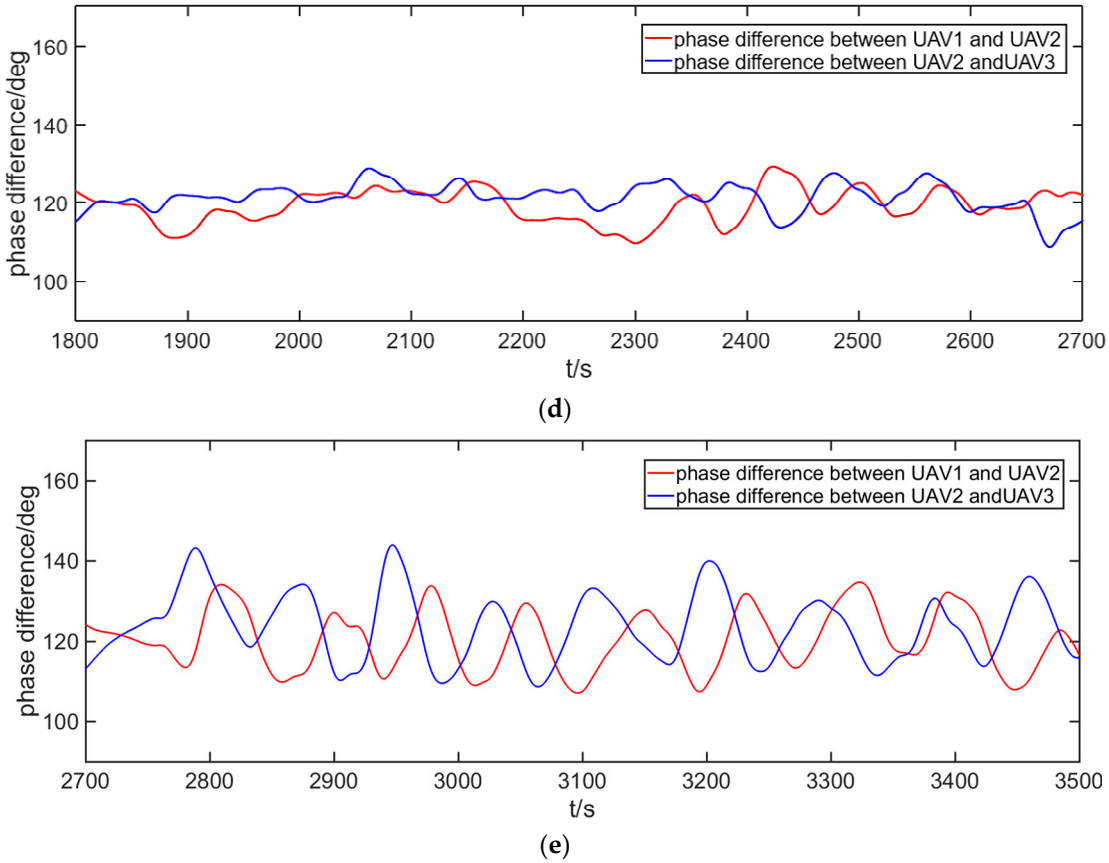

Figure 22. The phase difference. (**a**) Phase difference in the "gathering" stage; (**b**) Phase difference in the "phase adjusting" stage; (**c**) Phase difference in the "high-speed" stage; (**d**) Phase difference in the "low-speed" stage; (**e**) Phase difference in the "accelerating" stage.

6. Conclusions

This paper focused on the cooperative standoff tracking of moving targets. Three subproblems were discussed: Generating the optimal flyable path for a single UAV, standoff tracking of moving targets, and intervehicle phase keeping for cooperative tracking. For the first subproblem, we discussed the influence of guidance parameter c on the trajectory. The gradient descent method was utilized to search the optimal guidance parameter c. The ILVF was introduced to prevent the UAV from traversing the circle orbit. In the second subproblem, the IMM-UKF algorithm was introduced to fuse localization results from three UAVs. In this way, the state of the target was estimated and used for correcting the guidance law in standoff tracking of moving targets. At last, aiming to make a team of UAVs converge to the desired intervehicle phase, a speed-based controller was proposed. A series of numerical simulations on three subproblems were well-designed and performed to demonstrate the feasibility of the proposed algorithm. To demonstrate the usability in reality, we further carried out high-fidelity hardware-in-the-loop simulations.

There are some potential modifications on this study. As an uncertain factor, wind can be regarded as a disturbance to flight control. Actual flight using fixed-wing UAVs will be carried out to verify the validity of our algorithm in more complex conditions.

Author Contributions: **Conceptualization,** J.L..**; data analysis,** F.C., J.L.**; writing-original draft preparation,** F.C.**; writing-review and editing,** F.C., J.L.**; supervision,** Y.N.**; project administration,** Y.N.**; funding acquisition, L.W. All authors have read and agreed to the published version of manuscript.**

Funding: This research was funded by The National Natural Science Foundation of China (No. 61876187).

Conflicts of Interest: The authors declare no conflict of interest.

Appendix A

(1) Information allocation

$$\begin{cases} Q_i(k) = \beta_i^{-1} Q_g(k) \\ P_i(k) = \beta_i^{-1} P_g(k) \\ \widehat{X}_i(k) = \widehat{X}_g(k) \\ \beta_i = \left(\left\|P_i(k \mid k)\right\|_{\mathrm{F}}\right)^{-1} \Big/ \sum \left(\left\|P_i(k \mid k)\right\|_{\mathrm{F}}\right)^{-1} \\ \beta_m = 0 \end{cases}$$

where $\beta_i (i = 1, 2, \cdots n)$ denotes the weights of local filters. β_m means the main filter. $Q_g(k)$ and $P_g(k)$ are separately the process noise and global mean square error matrix.

(2) Prediction and Update

In this step, the IMM-UKF is used to get the predicted state variables $X_i(k+1)$ and estimation covariance $P_i(k+1)$.

(3) Overall optimization

$$\begin{cases} \widehat{X}_g(k+1) = P_g(k+1) \sum P_i^{-1}(k+1) \widehat{X}_i(k+1) \\ P_g(k+1) = (\sum P_i^{-1}(k+1))^{-1} \end{cases}$$

The process above is a rough process to fuse the data from local filters. Detailed principle can be found in [25].

Appendix B

Assuming that n motion models are set in the IMM algorithm, of which the state equitation is

$$X_j[k+1] = A_j X_j[k] + \omega_j[k] \quad j = 1, 2 \cdots n$$

There are four steps in a typical iteration of the IMM algorithm: (1) Model interacting, (2) parallel filtering, (3) model update, (4) estimation output.

(1) Model interacting: Compute:

$$\hat{X}_{0j}(k \mid k) = \sum_{i=1}^{r} \hat{X}_i(k \mid k) \mu_{ij}(k \mid k)$$

$$\mu_{ij}(k \mid k) = p_{ij} \mu_i(k) \Big/ \bar{c}_j$$

$$\bar{c}_j = \sum_{i=1}^{r} p_{ij} \mu_i(k) \ , j = 1, \cdots, r$$

(2) Parallel filtering:

In this step, an unscented Kalman filter is used in parallel filtering. n motion model-based filters work in parallel to calculate the state estimation $\hat{X}_j(k+1)$ at time $k+1$ and the covariance estimation $P_j(k+1)$, mean error $\nu_j(k+1)$ and error covariance estimation $S_j(k+1)$.

(3) Model update:

$$\Lambda_j(k) = \frac{1}{(2\pi)^{n/2} \left|S_j(k)\right|^{1/2}} \exp\left\{-\frac{1}{2} \nu_j^T S_j^{-1}(k) \nu_j\right\}$$

$$\nu_j(k+1) = Z(k+1) - H(k+1) \hat{X}_j(k+1 \mid k)$$

$$S_j(k+1) = H(k+1)P_j(k+1|k)H(k+1)^T + R(k+1)$$

$$\mu_j(k+1) = \Lambda_j(k+1)\bar{c}_j \Big/ \sum_{j=1}^{r} \Lambda_j(k+1)\bar{c}_j$$

(4) Estimation output:

$$\hat{X}(k+1|k+1) = \sum_{j=1}^{r} \hat{X}_j(k+1|k+1)\mu_j(k+1)$$

$$P(k+1|k+1) = \sum_{j=1}^{r} \mu_j(k+1)\{P_j(k+1|k+1) + \left[\hat{X}_j(k+1|k+1) - \hat{X}(k+1|k+1)\right]\left[\hat{X}_j(k+1|k+1) - \hat{X}(k+1|k+1)\right]^T\}$$

The IMM-UKF is applied as the sub-filters in the federated filter to improve estimation performance for nonlinear systems, and the main filter is designed as [25].

References

1. Rysdyk, R.; Lum, C.; Vagners, J. Autonomous orbit coordination for two unmanned aerial vehicles. In Proceedings of AIAA Guidance, Navigation, and Control Conference and Exhibit; p. 6362.
2. Kim, S.; Oh, H.; Tsourdos, A.J.J.o.G., Control,; Dynamics. Nonlinear model predictive coordinated standoff tracking of a moving ground vehicle. 2013, 36, 557-566.
3. Oh, H.; Kim, S.; Tsourdos, A.J.I.T.o.A.; Systems, E. Road-map–assisted standoff tracking of moving ground vehicle using nonlinear model predictive control. 2015, 51, 975-986.
4. Wang, S.; Wei, R.; Lv, M. Unmanned aerial vehicle standoff target tracking using modified reference point guidance. In Proceedings of Proceedings of 2014 IEEE Chinese Guidance, Navigation and Control Conference; pp. 2381-2386.
5. Xu, Z.; Wei, R.; Zhao, X.; Wang, S.J.I.A. Coordinated Standoff Target Tracking Guidance Method for UAVs. 2018, 6, 59853-59859.
6. Dale, L. Lyapunov vector fields for UAV flock coordination. In Proceedings of presented at the 2nd AIAA "Unmanned Unlimited" Conf, and Workshop & Exhibit.
7. Frew, E.W.; Lawrence, D.A.; Morris, S.J.J.o.g., control,; dynamics. Coordinated standoff tracking of moving targets using Lyapunov guidance vector fields. 2008, 31, 290-306.
8. Chen, H.; Chang, K.; Agate, C.S.J.I.T.o.A.; Systems, E. UAV path planning with tangent-plus-Lyapunov vector field guidance and obstacle avoidance. 2013, 49, 840-856.
9. Oh, H.; Kim, S.; Tsourdos, A.; White, B.A.J.J.o.I.; Systems, R. Decentralised standoff tracking of moving targets using adaptive sliding mode control for UAVs. 2014, 76, 169-183.
10. Lim, S.; Kim, Y.; Lee, D.; Bang, H.J.J.o.I.; Systems, R. Standoff target tracking using a vector field for multiple unmanned aircrafts. 2013, 69, 347-360.
11. Pothen, A.A.; Ratnoo, A.J.J.o.G., Control,; Dynamics. Curvature-constrained Lyapunov vector field for standoff target tracking. 2017, 40, 2729-2736.
12. Sun, S.; Wang, H.; Liu, J.; He, Y.J.I.A. Fast Lyapunov Vector Field Guidance for Standoff Target Tracking Based on Offline Search. 2019, 7, 124797-124808.
13. Modirrousta, A.; Sohrab, M.; Dehghan, S.M.M.J.T.o.t.I.o.M.; Control. A modified guidance law for ground moving target tracking with a class of the fast adaptive second-order sliding mode. 2016, 38, 819-831.
14. Park, S.J.J.o.G., Control,; Dynamics. Guidance law for standoff tracking of a moving object. 2017, 40, 2948-2955.
15. Summers, T.H.; Akella, M.R.; Mears, M.J.J.J.o.G., Control,; Dynamics. Coordinated standoff tracking of moving targets: Control laws and information architectures. 2009, 32, 56-69.
16. Qian, Z.; Rui, Z.; Jie, Z. Coordinated standoff tracking of moving targets with optimal measurement configuration. In Proceedings of 2016 13th International Computer Conference on Wavelet Active Media Technology and Information Processing (ICCWAMTIP); pp. 468-472.
17. Hu, C.; Zhang, Z.; Tao, Y.; Wang, N.J.I.A. Decentralized real-time estimation and tracking for unknown ground moving target using UAVs. 2018, 7, 1808-1817.

18. Kingston, D.; Beard, R. UAV splay state configuration for moving targets in wind. In Advances in Cooperative Control and Optimization, Springer: 2007; pp. 109-128..
19. Song, Z.-q.; Li, H.-x.; Chen, C.-l.; Zhou, X.-z.; Xu, F.J.J.o.Z.U.S.C. Coordinated standoff tracking of moving targets using differential geometry. 2014, 15, 284-292.
20. Kokolakis, N.-M.T.; Koussoulas, N.T. Coordinated standoff tracking of a ground moving target and the phase separation problem. In Proceedings of 2018 International Conference on Unmanned Aircraft Systems (ICUAS); pp. 473-482.
21. He, S.; Wang, J.; Lin, D.J.P.o.t.I.o.M.E., Part G: Journal of Aerospace Engineering. Unknown ground moving target tracking using multiple unmanned aerial vehicles. 2019, 233, 1021-1032.
22. Wang, C.; Yan, C.; Xiang, X.; Zhou, H. A Continuous Actor-Critic Reinforcement Learning Approach to Flocking with Fixed-Wing UAVs. In Proceedings of Asian Conference on Machine Learning; pp. 64-79.
23. Yang, L.; Liu, Z.; Wang, X.; Xu, Y.J.I.A. An optimized image-based visual servo control for fixed-wing unmanned aerial vehicle target tracking with fixed camera. 2019, 7, 68455-68468.
24. Petritoli, E.; Giagnacovo, T.; Leccese, F. Lightweight GNSS/IRS integrated navigation system for UAV vehicles. In Proceedings of 2014 IEEE Metrology for Aerospace (MetroAeroSpace); pp. 56-61.
25. Yuan, G.; Yuan, K.; Zhang, H. A variable proportion adaptive federal kalman filter for INS/ESGM/GPS/DVL integrated navigation system. In Proceedings of 2011 Fourth International Joint Conference on Computational Sciences and Optimization; pp. 978-981.